Return

UCRL-16778

University of California

Ernest O. Lawrence Radiation Laboratory

DISLOCATION MECHANISMS IN SINGLE CRYSTALS
OF TANTALUM AND MOLYBDENUM AT LOW TEMPERATURES

DISCLAIMER

Submitted to Acta Metallurgica UCRL-16778

UNIVERSITY OF CALIFORNIA
Lawrence Radiation Laboratory
Berkeley, California

AEC Contract No. W-7405-eng-48

DISLOCATION MECHANISMS IN SINGLE CRYSTALS OF TANTALUM AND MOLYBDENUM AT LOW TEMPERATURES

S. S. Lau, S. Ranji, A. K. Mukherjee, G. Thomas and J. E. Dorn

March 1966

UCRL-16778

UNIVERSITY OF CALIFORNIA

Lawrence Radiation Laboratory
Berkeley, California

DISLOCATION MECHANISMS IN SINGLE CRYSTALS OF TANTALUM AND MOLYBDENUM AT LOW TEMPERATURES

S. S. Lau,[1] S. Ranji,[2] A. K. Mukherjee,[3] G. Thomas[4] and J. E. Dorn[5]

March, 1966

[1,2]Research Assistants, Inorganic Materials Research Division, Lawrence Radiation Laboratory, University of California, Berkeley, California.

[3]Post-Doctoral Fellow, Inorganic Materials Research Division, Lawrence Radiation Laboratory, University of California, Berkeley, California (currently Senior Scientist, Metal Science Group, Battelle Memorial Institute, Columbus, Ohio).

[4,5]Professors of Metallurgy and Materials Science, respectively, Department of Mineral Technology, College of Engineering and Research Metallurgists, Inorganic Materials Research Division, Lawrence Radiation Laboratory, University of California, Berkeley, California.

ABSTRACT

High purity single crystals of Ta and Mo oriented for $(\bar{1}01)$ [111] single slip were tested in tension over the range of temperatures up to 620°K at two strain rates. Activation energies and activation volumes were determined. Analyses of the data revealed that they were in good agreement with the Peierls mechanism.

I. INTRODUCTION

The deformation characteristics of most b.c.c. metals at low temperatures differ markedly from those exhibited by f.c.c. metals,[1] for example: (a) The yield strength and flow stress of b.c.c. metals increase rapidly with decreasing temperatures and with increasing strain rates in contrast to the much more modest trends exhibited by f.c.c. metals. (b) The activation volume for deformation of b.c.c. metals is in the range of 5 to $50b^3$ (b = Burgers' vector) whereas that for f.c.c. metals is often 100 to 10 times larger. (c) The activation volume of b.c.c. metals is independent of strain while that for f.c.c. metals decreases with increasing strains. (d) The increase in the yield stress with decrease in temperature is independent of the strain-hardened state in b.c.c. metals whereas it is greater for the higher strain-hardened states in f.c.c. metals. (e) Although the deformation characteristics of f.c.c. metals at low temperatures agree well in all details with the requirements of the intersection model, those for b.c.c. metals cannot be rationalized on this basis.

Over the past few years several different thermally activated dislocation mechanisms have been proposed to account for the unique behavior of b.c.c. metals at low temperatures. In summary, these are: (a) Interaction of dislocations with interstitial impurity atoms or with substitutional solute atoms.[2,3] (b) Intersection of dislocations with clusters of foreign atoms.[4] (c) Resistance to the motion of dislocations due to jogs on screw dislocations.[5] (d) Resistance to the motion of dislocations due to the Snoeck effect.[6] (e) Interaction of dislocations with the intrinsic resistance to motion due to Peierls' hills.[1,7-9]

The aim of the present investigation was to determine the rate controlling mechanism of deformation in Ta and Mo at low temperatures. In order to eliminate or at least minimize the possible operation of some of the previously suggested mechanisms (a, b and d mentioned above), only high purity zone refined metals were used. In addition it was considered advisable to investigate in detail oriented single crystals so as to eliminate complications that might arise in the interpretation of the data due to possible auxiliary grain size, polyslip and orientation effects.

II. EXPERIMENTAL TECHNIQUES

Commercially pure (1/4 in. in diameter) Ta and Mo rods were given two refining passes (at 4 mm/min) in a highly evacuated (below 10^{-6} torr) electron beam floating zone equipment. Such zone refined rods were then given two additional passes following seeding of single crystals in

the selected orientation. Laue back-reflection x-ray diffraction technique was used to determine the Schmid angles, λo and χo, for $(\bar{1}01)$ [111] slip. The various orientations employed were within $\pm 2^\circ$ of that shown in the stereographic projection of Fig. 1 so selected as to maximize the possibility of slip on the $(\bar{1}01)$ plane and minimize the possibility of slip on the $(12\bar{3})$ and $(\bar{1}12)$ planes. Only $(\bar{1}01)$ [111] slip traces were observed on the free surface following tensile straining.

Tensile specimens 1.75 in. long having a gauge section 0.80 in. long and 0.100 in. in diameter were prepared by carefully machining the single crystal rods. Each specimen was then electropolished at 0°C to remove about 200 microns so as to reduce possible effects of residual machining stresses. Specific resistivity measurements were made at 273°, 77° at 4.2°K as a check on the purity with the following results

	Ta	Mo
$\frac{\rho 273^\circ}{\rho 4.2^\circ}$	$\sim 10^4$	$\sim 10^3$

which indicates that the crystals are of quite high purity.

Tensile tests were conducted in an Instron Testing Machine at a series of temperatures. Two strain rates were used and test temperatures were within $\pm 1^\circ$K of the reported values; the stresses were accurate to $\pm 3 \times 10^6$ dynes/cm^2, and tensile strains were measured to within an accuracy of ± 0.001.

III. EXPERIMENTAL RESULTS

Preliminary tension tests revealed that the deformation mechanism

at 550°K was athermal for both Ta and Mo. In order to reduce the scatter in the single crystal flow stresses, specimens were prestrained to about a strain of 0.15 at 550°K to attempt to achieve a standard work-hardened state, as follows:

Metal	Strain Rate (per sec)	Standard Flow Stress dynes/cm^2
Ta	9.6×10^{-5}	1.40×10^{8}
Mo	9.15×10^{-5}	3.11×10^{8}

Following prestraining each specimen was unloaded and the yield strength at 0.2% offset was determined at the desired temperature and strain rate as shown in Fig. 2. Ta twinned and fractured for $\dot{\gamma} = 8.05 \times 10^{-5}$ per sec at 4.2°K and for $\dot{\gamma} = 8.05 \times 10^{-3}$ per sec at 78°K. The reported datum points connected by the solid lines in Fig. 2, however, refer to reliable yield strengths of crystals free of twinning.

Over the higher temperature ranges both Ta and Mo exhibited an athermal behavior where the flow stress was insensitive to both strain rate and temperature. In the lower temperature range the flow stress of both metals increased rapidly as the temperature was decreased or as the strain rate was increased, revealing the operation of a thermally activated mechanism of deformation.

The total measured flow stress, τ, arises from the sum of the athermal component, τ_A, and the thermally sensitive component, τ^*. Since the athermal component depends on long range interactions between dislocations it varys with temperature as does the shear modulus of

elasticity according to

$$\tau_{A(T)} = \frac{\tau_{A(550)} G_T}{G(550)} \qquad (1)$$

where the subscripts refer to the temperature and G is the shear modulus of elasticity. Correspondingly the thermally sensitive flow stress is then given by

$$\tau^* = \tau - \tau_{A(T)} \qquad (2)$$

Values of G versus T for shear on the $(\bar{1}10)$ plane in the [111] direction were calculated from the single crystal data of Featherstone and Neighbours[10] for Ta (G_o = .658 x 10^{12} dynes/cm^2) and from the data of Bolef and DeKlerk[11] for Mo (G_o = 1.372 x 10^{12}dynes/cm^2). The effect of temperature on τ^*, as determined from Eq. (2), is shown in Fig. 3.

At low temperatures thermally activated dislocation mechanisms usually obey the empirical relationship suggested by the Boltzmann expression, namely,

$$\dot{\gamma} = \dot{\gamma}_o \, e^{\frac{-U\{\tau^*\}}{kT}} \qquad (3)$$

where the activation energy $U\{\tau^*\}$ is a function of τ^* and varies with temperature as does the shear modulus such that

$$U\{\tau^*\} = U_o\{\tau^*\} \, (G_T/G_o) \qquad (4)$$

where $U_o\{\tau^*\}$ refers to what the activation energy would have been if the shear modulus were that at the absolute zero. For some mechanisms, such as the intersection process, $U\{\tau^*\}$ also depends on the dislocation

arrangements[12] and substructure, but for other mechanisms, such as the Peierls process, $U\{\tau^*\}$ is independent of the substructure.[1,13] The value of the standard strain rate, $\dot{\gamma}_o$, always depends on the density of mobile dislocations; it may also depend on the substructure but it is generally insensitive to changes in T and τ^*. The apparent activation energies, defined by,

$$q = -\left(\frac{\partial \ell n \dot{\gamma}}{\partial\, 1/kT}\right)_{\tau^*} = -\left(\frac{\partial \ell n \dot{\gamma}_o}{\partial\, 1/kT}\right)_{\tau^*} + \frac{\partial}{\partial \frac{1}{kT}}\left(\frac{U}{kT}\right)_{\tau^*} \simeq \frac{\partial}{\partial\, 1/kT}\left(\frac{U}{kT}\right)_{\tau^*} \qquad (5)$$

were determined from Fig. 3 and are recorded in Fig. 4. Whereas q usually decreases linearly with increasing τ^* for the intersection mechanism (especially when dislocations are undissociated) both Ta and Mo give somewhat curve-linear trends, suggestive of the Peierls mechanism. A more definitive judgement, however, can be based on the apparent activation volume, v, defined by

$$v = kT\left(\frac{\partial \ell n \dot{\gamma}}{\partial \tau^*}\right)_T = kT\left(\frac{\partial \ell n \dot{\gamma}_o}{\partial \tau^*}\right)_T - \left(\frac{\partial U}{\partial \tau^*}\right)_T \simeq \left(\frac{\partial U}{\partial \tau^*}\right)_T \qquad (6)$$

The activation volumes, as deduced from Fig. 3 are recorded in Fig. 5. These activation volumes are not only much smaller than those obtained by the intersection mechanism but, unlike those for intersection, which are usually independent of τ^*, the activation volumes for Ta and Mo decrease with increasing τ^*; these trends strongly infer the operation of the Peierls process. Additional confirmation of the operation of the Peierls process is shown in Fig. 6 which gives the activation volumes deduced by rapid changes in strain rate during the course of

straining at one temperature. The values given at $\gamma = 0$ refer to those deduced from the data of Fig. 3. Whereas these activation volumes are independent of strain-hardening and agree with the corresponding activation volumes deduced from Fig. 3, those for intersection would have decreased with increased straining.

IV. DISCUSSION

In this section a detailed analysis of the previously described low temperature deformation characteristics of Ta and Mo will be made in an attempt to ascertain whether indeed all details agree well with expectations based on the Peierls mechanism. Various models[12-20] have been suggested in the past for the Peierls process. We shall, however, confine our attention exclusively to the Dorn-Rajnak model,[21] since it has been shown to agree well with carefully obtained experimental facts for $(12\bar{3})$ [111] slip in the CsCl lattice of AgMg,[22] for prismatic slip in the hexagonal Ag-33 at.% Al alloy,[23] and for deformation of polycrystalline Fe below about 160°K.[24,25]

The model assumes that the line energy $\Gamma\{y\}$ of a dislocation varies periodically along parallel rows of atoms on the slip plane according to

$$y = \frac{\Gamma_c - \Gamma_o}{2} + \frac{\Gamma_c - \Gamma_o}{2}\left\{\frac{\alpha}{2} + \cos 2\pi \frac{y}{a} - \frac{\alpha}{4}\cos\frac{4\pi y}{a}\right\} \qquad (7)$$

where Γ_c is the line energy at $y = 0$, Γ_o at $y = \pm a/2$, a is the period of the hills and α which can vary from -1 to +1 perturbs the shape of the hills from a purely sinusoidal variation given when $\alpha = 0$. The Peierls stress τ_p is the maximum stress that need be applied to move,

without the aid of a thermal fluctuation, a dislocation from one valley to the next and is given by

$$\tau_p b = \frac{\Gamma_c - \Gamma_o}{|\alpha| a} \frac{\alpha}{16} \left(3 + \sqrt{1 + 8\alpha^2}\right) \left(\sqrt{8\alpha^2 - 2 + 2\sqrt{1 + 8\alpha^2}}\right) \quad (8)$$

The Peierls stress, therefore, is the stress τ_p^o needed to initiate deformation at absolute zero. Since the Peierls stress depends on the line energy, it changes with temperature as does the shear modulus of elasticity according to $\tau_p = \tau_p^o \, G/G_o$ (see e.g., Friedel[12]) when a stress τ^* which is less than τ_p is applied, the dislocation moves partway up the Peierls hill to y_o where

$$\tau^* b = - \frac{\pi}{a} (\Gamma_c - \Gamma_o) \sin \frac{2\pi y_o}{a} \left(1 - \alpha \cos \frac{2\pi y_o}{a}\right) \quad (10)$$

At absolute zero no further motion can take place but at higher temperatures thermal fluctuations assist in nucleating pairs of kinks. Such fluctuations cause segments of dislocations to bow out. As they bow out their line energy increases and the applied stress does work equal to $\tau^* b$ times the area swept out. The total energy at first increases but finally it reaches a maximum critical value and then decreases. All thermal fluctuations having energy greater than this critical energy U_n result in nucleation of a pair of kinks. The critical value of U_n was determined using the calculus of variations and numerical analyses gave

$$\tau^*/\tau_p = f(U_n/2U_k) \quad (11)$$

where U_k is the energy of a single complete kink as shown by the curves in Figs. 7a, 7b and 8.

The true activation volume, defined as

$$v^* = -\frac{\partial U}{\partial \tau^*} = \frac{-2U_k \, \partial(U_n/2U_k)}{\tau_p \, \partial(\tau^*/\tau_p)} \tag{12}$$

is shown by the curves in Fig. 9, and the theoretical relationship between the Peierls stress, kink energy and line energy is given in Fig. 10. Variations in the shape of the Peierls hills (over the range $-1 \leq \alpha \leq 1$) has only a modest influence on the correlations.

The shear strain rate is given by

$$\dot{\gamma} = \rho ab \, \frac{\nu L}{w} \, e^{\frac{-U_n}{kT}} \tag{13}$$

where ρ is the density of mobile dislocations, ν is the Debye frequency, L the distance over which the kinks move before they become arrested and w is the width of the critical kink loop. The above formulation assumes that only one pair of kinks is nucleated and moving at one time in the segment of length L. Other assumptions such as the simultaneous nucleation of several pairs of kinks[21] lead to formulations that are not in agreement with past or current experimental facts. Although $\rho L/w$ may depend on τ^* the correlations achieved to date and that which follows here suggest that $\rho L/w$ is substantially a constant for a given metal and strain-hardened state.

As shown in Fig. 8 when τ^* equals zero, $U_n = 2U_k$; this first occurs at a critical temperature T_c. Consequently

$$\dot{\gamma} = \rho ab \, \frac{\nu L}{w} \, e^{\frac{-2U_k}{kT_c}} \tag{14}$$

and therefore, for the same values of $\dot{\gamma}$ and $\rho L/w$,

$$\frac{\tau^*}{\tau_p} = \frac{\tau^*}{\tau_p^\circ}\,(G_c/G_T) = f\left(\frac{U_n}{2U_k}\right) = f(T/T_c) \tag{15}$$

as shown by dividing Eq. (13) by (14) and introducing the results into Eq. (11). Here τ_p° refers to the Peierls stress at absolute zero and the Peierls stress is assumed to change with temperature linearly with the shear modulus of elasticity. Thus the abcissae of Fig. 7a and Fig. 7b are also equal to T/T_c where T_c is the critical temperature at which τ^* first becomes zero. The kink energy at the absolute zero, U_k° can be obtained from the values of the critical temperatures at two strain rates, namely,

$$\frac{\dot{\gamma}_1}{\dot{\gamma}_2} = \frac{e^{\frac{-2U_k^\circ}{kTc_1}\left(\frac{G}{G_{Tc_1}}\right)}}{e^{\frac{-2U_k^\circ}{kTc_2}\left(\frac{G_o}{G_{Tc_2}}\right)}} \tag{16}$$

Two features of Fig. 3 prevent a simple direct analyses of these data. First it is not easily possible to extrapolate these data to the absolute zero in order to obtain τ_p°; secondly the values of T_c at which $\tau^* = 0$ cannot be determined accurately. To overcome these difficulties $\tau^*(G_o/G_T)$ was plotted as a function of T on logarithmic scales and then superimposed over the analogous theoretical plot of τ^*/τ_p versus $U_n/2U_k$ so as to obtain coincidence between experiment and theory as shown in Figs. 7a and 7b. From these curves the values of τ_p°, and T_c and α were determined as shown in Table 1.

The kink energies, U_k^o were calculated by means of Eq. (16) and the line energies Γ^o at the absolute zero were determined from τ_p^o and U_k^o using the correlations given in Fig. 10.

A correlation between theory and experiment is given in Fig. 8. The experimental datum points of τ^*/τ_p versus $U_n/2U_k = T/T_c$ were calculated from the original data using the values of τ_p^o and U_k^o as deduced in Table 1. The lines refer to the theoretically determined relationships for the Peierls process. In general the agreement is very good. One small point of discrepancy concerns the fact that τ^*/τ_p at the two lower temperature points for Ta appear to be somewhat higher than the theoretical model predicts. In view of the care exercised this does not appear to be ascribable to experimental error. Rather this effect might arise from the possibility that the Peierls hill in Ta is initially somewhat steeper than any of the range of slightly modified sinusoidal hills that were assumed in the theory. As will be shown, the activation volumes for Ta in this region are completely in harmony with the requirements of the Peierls mechanisms; consequently this discrepancy is deemed to be of secondary importance. A second point of minor discrepancy is noted for Mo where the values of τ^*/τ_p seem to decrease more slowly as T approaches T_c than the current models predict. In contrast the Ta data and the previously reported results for AgMg and Ag_2Al[22,23] did not exhibit this anomalous behavior. A much more pronounced discrepancy between theory and experiment in this region has been noted for the case of polycrystalline Fe[25] containing Mn. In the case of Fe the activation volumes in the high temperature

region are orders of magnitude higher than those that are reasonable for a Peierls mechanism. In the case of Mo reported here, however, the activation volumes, as will be shown, are consistent with expectations based on the Peierls mechanism. It is unlikely that the slightly anomalous trend for Mo in this region is ascribable to experimental error; it might arise from the possibility that the Peierls valley is somewhat broader than assumed in the theoretical model. Thus we conclude that τ^*/τ_p versus T/T_c data for Ta and Mo are in good agreement with the Peierls mechanism over the entire low temperature range investigated here.

The most distinctive characteristic of the Peierls mechanism is its small activation volume which is independent of strain and increases as τ^* decreases. The independence of the activation volume for Ta and Mo on strain is documented in Fig. 6. The effect of τ^*/τ_p on the activation volume is given by Eq. (12) and the theoretically deduced curves of Fig. 9. The experimental datum points shown in Fig. 9 were calculated using the values of τ_p and U_k deduced in Table 1. Although the experimental points exhibit some scatter, they cluster, as well as can be expected in terms of experimental variations in $\Delta\tau^*$ with $\Delta\dot{\gamma}$ and the theoretically assumed shapes of the Peierls hills, about the theoretical curves to provide unequivocable confirmation of the operation of the Peierls mechanism.

Further confirmation of the Peierls mechanism is given in Table 1 where the line energy Γ^o deduced from the Peierls stress and the kink energy can be compared with Nabarro's isotropic estimate of $G_o b^2/2$ for

this quantity. Inasmuch as the Ta and Mo are elastically anisotropic and the estimate of $G_o b^2/2$ is very crude, the agreement is good and strengthens the belief that the Peierls mechanism is operative. Furthermore the values of $\rho L/w$ given in Table 1 are within the acceptable range.

CONCLUSIONS

(1) High purity single crystals of Ta and Mo oriented for $(\bar{1}01)$ [111] slip exhibit a thermally activated deformation mechanism at low temperatures.

(2) The following types of data confirm the operation of the Peierls mechanism:

   (a) Stress-temperature relationship.

   (b) Activation volume versus stress.

   (c) Activation volume versus strain.

   (d) The deduced kink energy.

   (e) The deduced line energy of a dislocation.

(3) The Peierls stress was estimated to be 33×10^8 dynes/cm^2 for Ta and 42×10^8 dynes/cm^2 for Mo.

REFERENCES

1. H. Conrad, Nat. Phys. Lab. Symposium on the Relation between the Structure and Mechanical Properties of Metals, Her Majesty's Stationery Office, London, 475 (1963).

2. D. F. Stein, J. R. Low and A. V. Seybolt, Acta Met., 11, 1253 (1963).

3. R. L. Fleischer, Acta Met., 10, 835 (1962).

4. B. L. Mordike and P. Haasen, Phil. Mag., 7, 459 (1962).

5. G. Schoeck, Acta Met., 9, 382 (1961).

6. G. Schoeck, Phys. Rev., 102, 1458 (1956).

7. H. Conrad and W. Hayes, Trans. ASM, 56, 125 (1963).

8. J. Heslop and N. J. Petch, Phil. Mag., 1, 866 (1956).

9. Z. S. Basinski and J. W. Christian, Aust. Jul. Phys., 13, 299 (1960).

10. F. H. Featherstone and J. R. Neighbours, Phys. Rev., 130, 1324 (1963).

11. G. U. Bolef and L. R. DeKlerk, J. Appl. Phys., 33, (7) 2311 (1962).

12. J. Friedel, Dislocations, Addison-Wesley Publishing Co., Reading, Mass., 1964.

13. A. Seeger, Phil. Mag., 1, 651 (1956).

14. A. Seeger, H. Donth and F. Pfaff, Discussions Faraday Soc., No. 23, 19 (1957).

15. A. Seeger and P. Schiller, Acta Met., 10, 348 (1962).

16. J. Lothe and J. P. Hirth, Phys. Rev., 1959, 115, 543 (1959).

17. T. Jossang, K. Skylstad and J. Lothe, National Physical Laboratory, Teddington, Middlesex, England, January, 1963.

18. J. Friedel, Electron Microscopy and Strength of Crystals, G. Thomas and J. Washburn, eds., 605 Interscience Publishers, 1963.

19. A. D. Brailsford, Phys. Rev., 122, 778 (1961) part I, and Phys. Rev., 128, 1033 (1962) part II.

20. V. Celli, M. Kabler, T. Miromiya and R. Thomson, Phys. Rev., 131, 58 (1963).

21. J. E. Dorn and S. Rajnak, Trans. AIME, 230, 1052 (1963).

22. A. K. Mukherjee and J. E. Dorn, Trans. AIME, 230, 1065 (1964).

23. A. Rosen, J. D. Mote and J. E. Dorn, Trans. AIME, 230, 1070 (1964).

24. A. Rosen, P. P. Wynblatt and J. E. Dorn, Trans. AIME, 233, 651 (1965).

25. P. P. Wynblatt and J. E. Dorn, "Dislocation Mechanisms in an Iron-Manganese Alloy at Low Temperatures, December, 1965, UCRL-16601.

FIGURE CAPTIONS

1. Orientation of the tensile axis of the crystal.
2. Flow stress vs. temperature.
3. Thermal sensitive component of the flow stress vs. temperature.
4. Apparent activation energy.
5. Apparent activation volume.
6. Apparent activation volume.
7. (a) The thermally activated flow stress vs. temperature for Mo.
   (b) Thermally activated flow stress vs. temperature in dimensionless time for Ta.
8. The thermally activated flow stress vs. temperature for Ta and Mo.
9. The thermally activated component of flow stress vs. activation volume in dimensionless time for Ta and Mo.
10. Variation of K with α for nucleation of dislocation kinks.

ACKNOWLEDGMENT

This report was prepared as part of the activities of the Inorganic Materials Research Division of the Lawrence Radiation Laboratory of the University of California, Berkeley, and was done under the auspices of the U. S. Atomic Energy Commission.

Table 1. Results of Analysis

Metal	$\dot{\gamma}$ per sec	α	τ_p^o dynes/cm^2	T_c ^oK	U_k^o ergs	Γ^o ergs/cm	$G_o(\bar{1}01)[111]$ x 10^{-12} dynes/cm^2	$G_o b^2/2$ ergs	$\frac{\rho L}{w}$ cm^{-2}
Ta	9.6×10^{-5} 8.05×10^{-5}	0	$33.4 \times 10^{+8}$	375 ± 15 490 ± 15	.5 ± .1 ± 10^{-12}	$.42 \times 10^{-3}$	.658	$.27 \times 10^{-3}$	5×10^8
Mo	9.9×10^{-5}sec^{-1} 9.15×10^{-3}	0	41.9×10^8	447 ± 15 518 ± 15	1.0 ± 2 x 10^{-12}	1.5 ± .1 x 10^{-3}	1.372	.51 x 10^{-3}	1.5 x 10^{11}

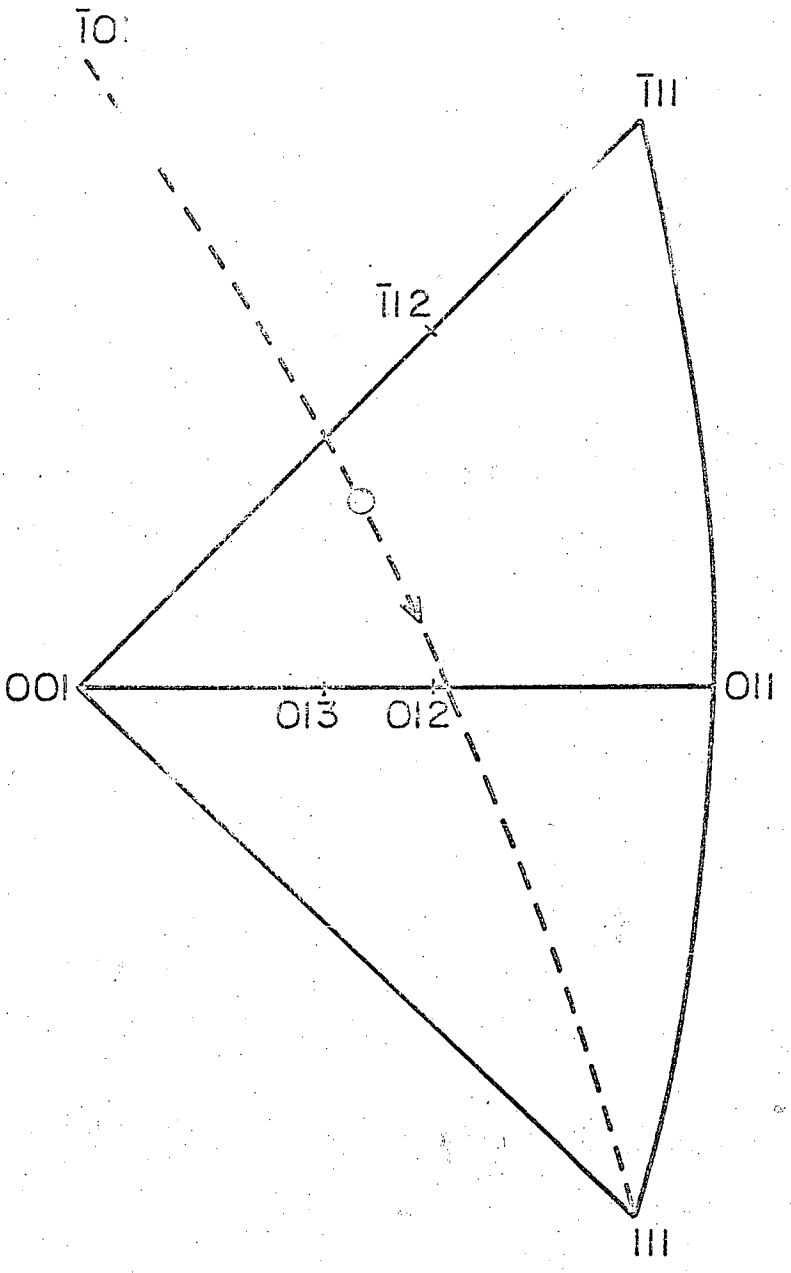

FIG. 1. ORIENTATION OF THE TENSILE AXIS OF THE CRYSTAL.

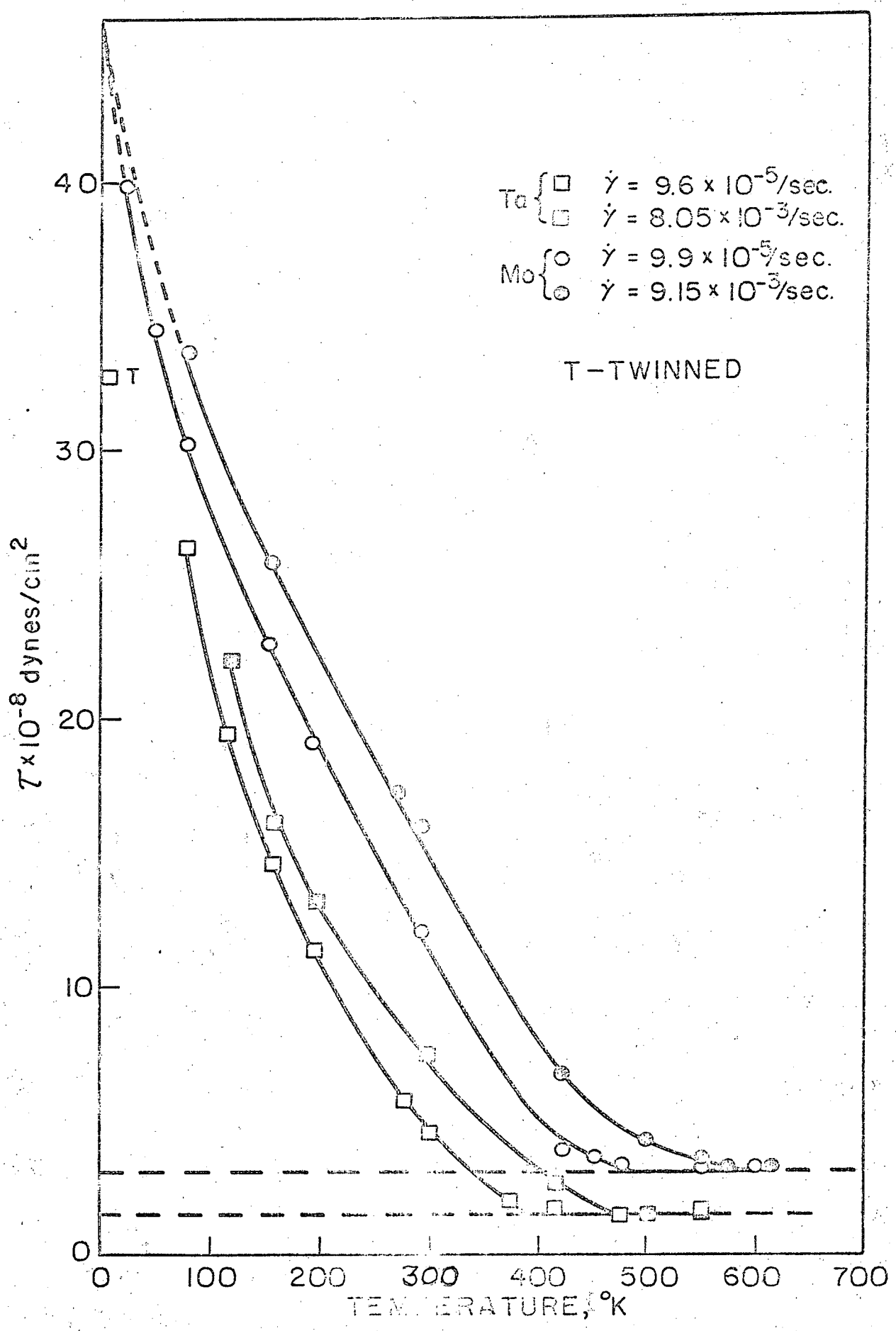

FIG. 2. FLOW STRESS vs. TEMPERATURE.

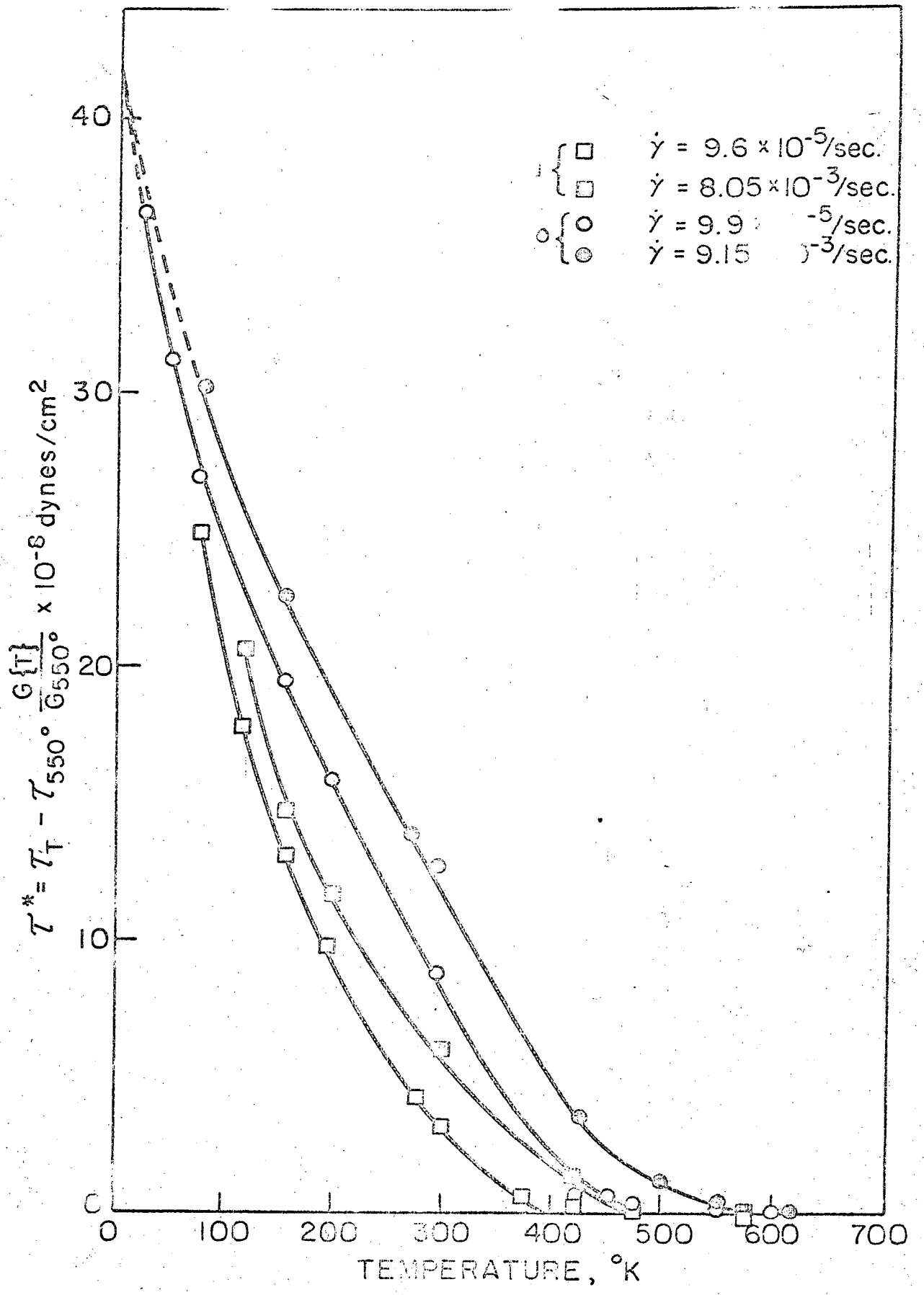

FIG. 3. THERMAL SENSITIVE COMPONENT OF THE FLOW STRESS vs. TEMPERATURE

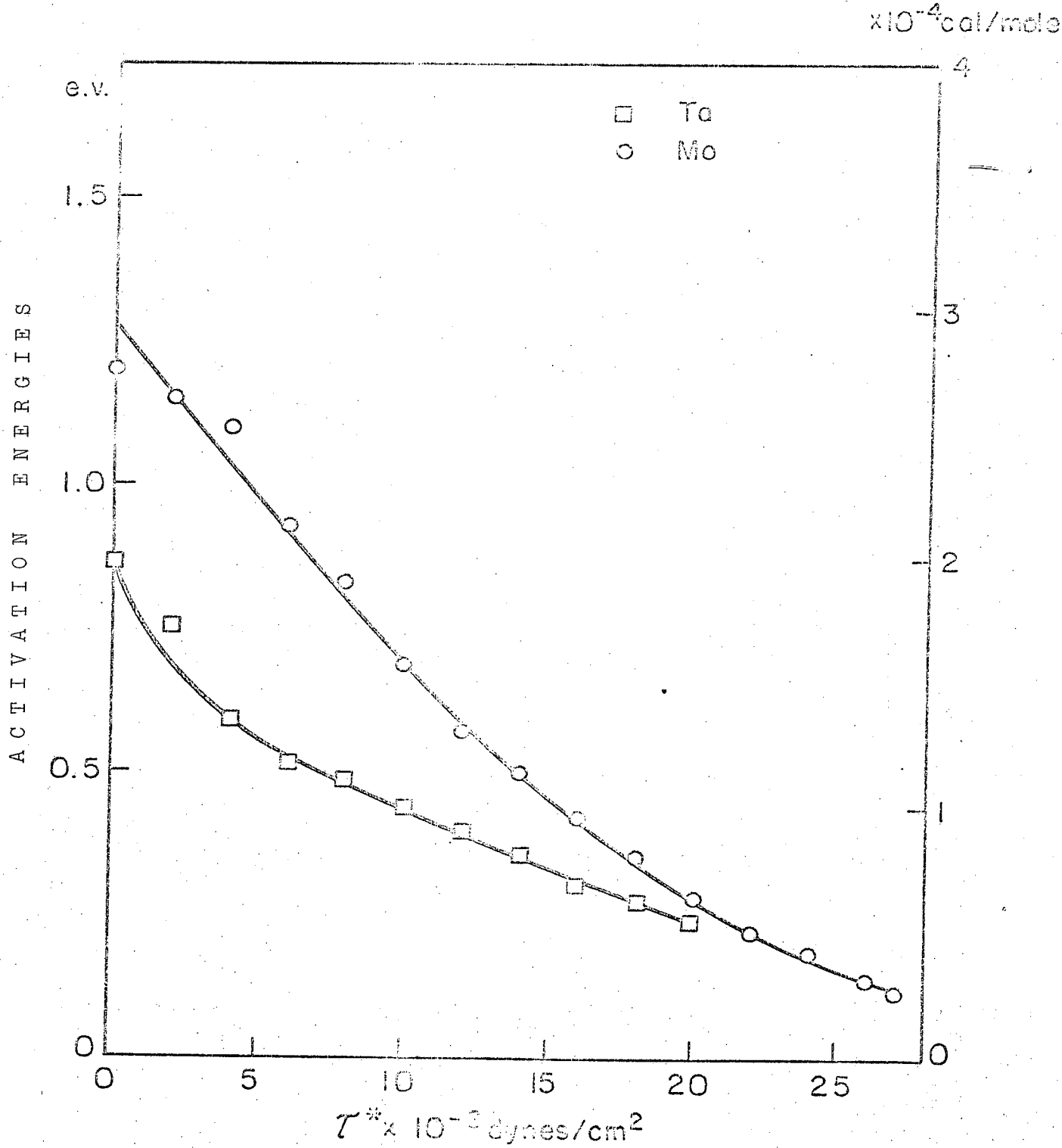

FIG. 4. APPARENT ACTIVATION ENERGY

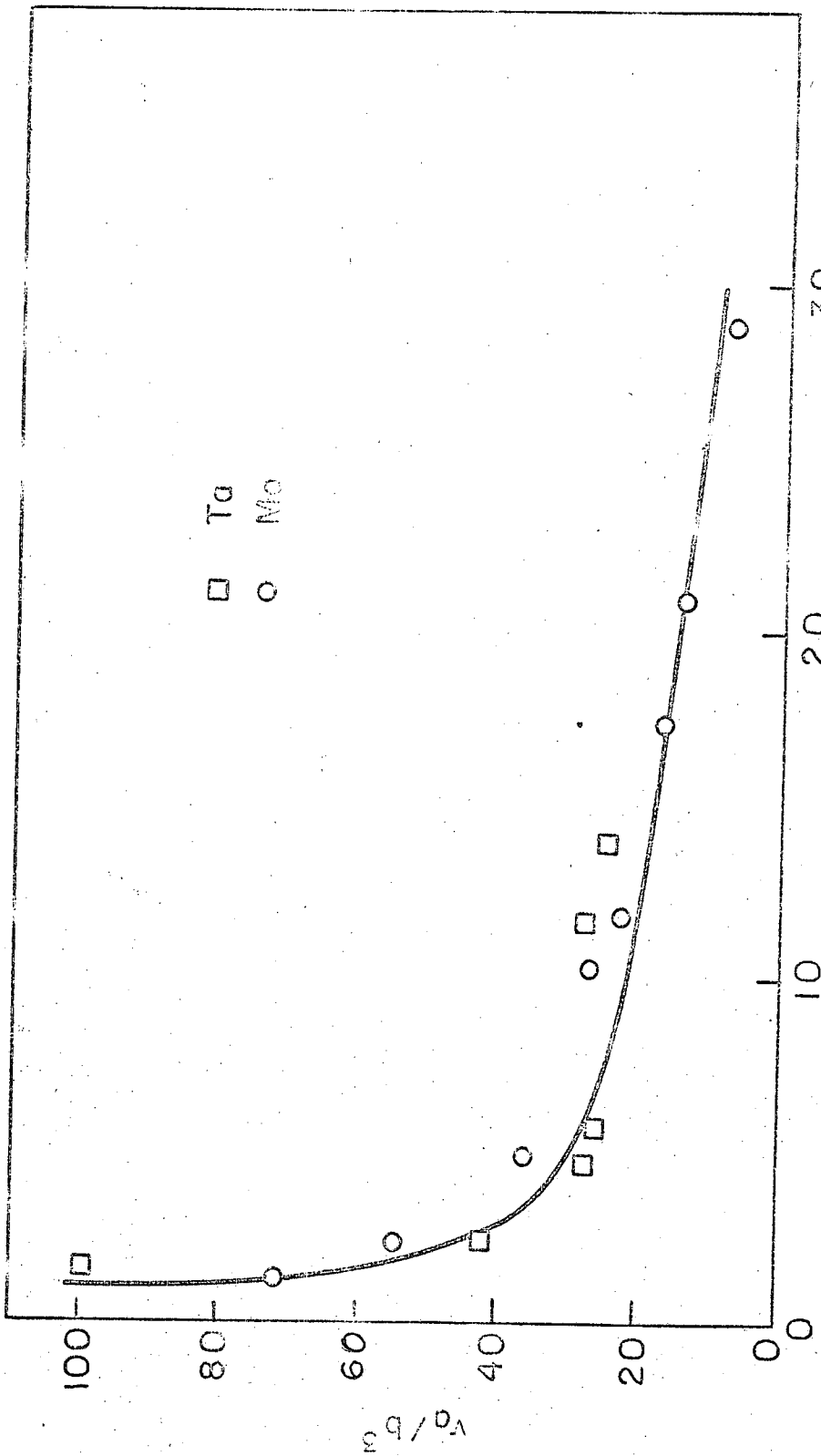

FIG. 5. APPARENT ACTIVATION VOLUME.

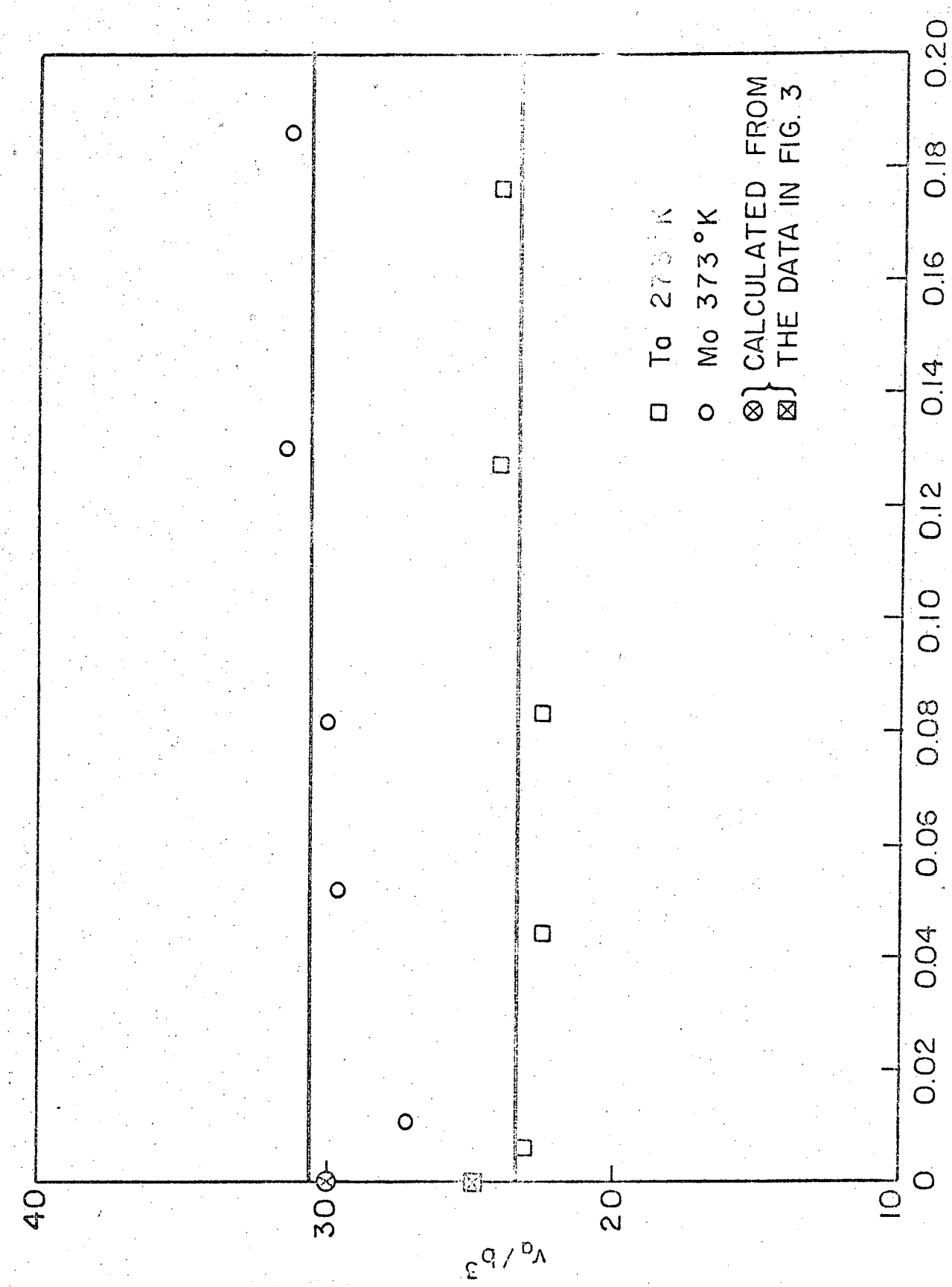

FIG. 6. APPARENT ACTIVATION VOLUME.

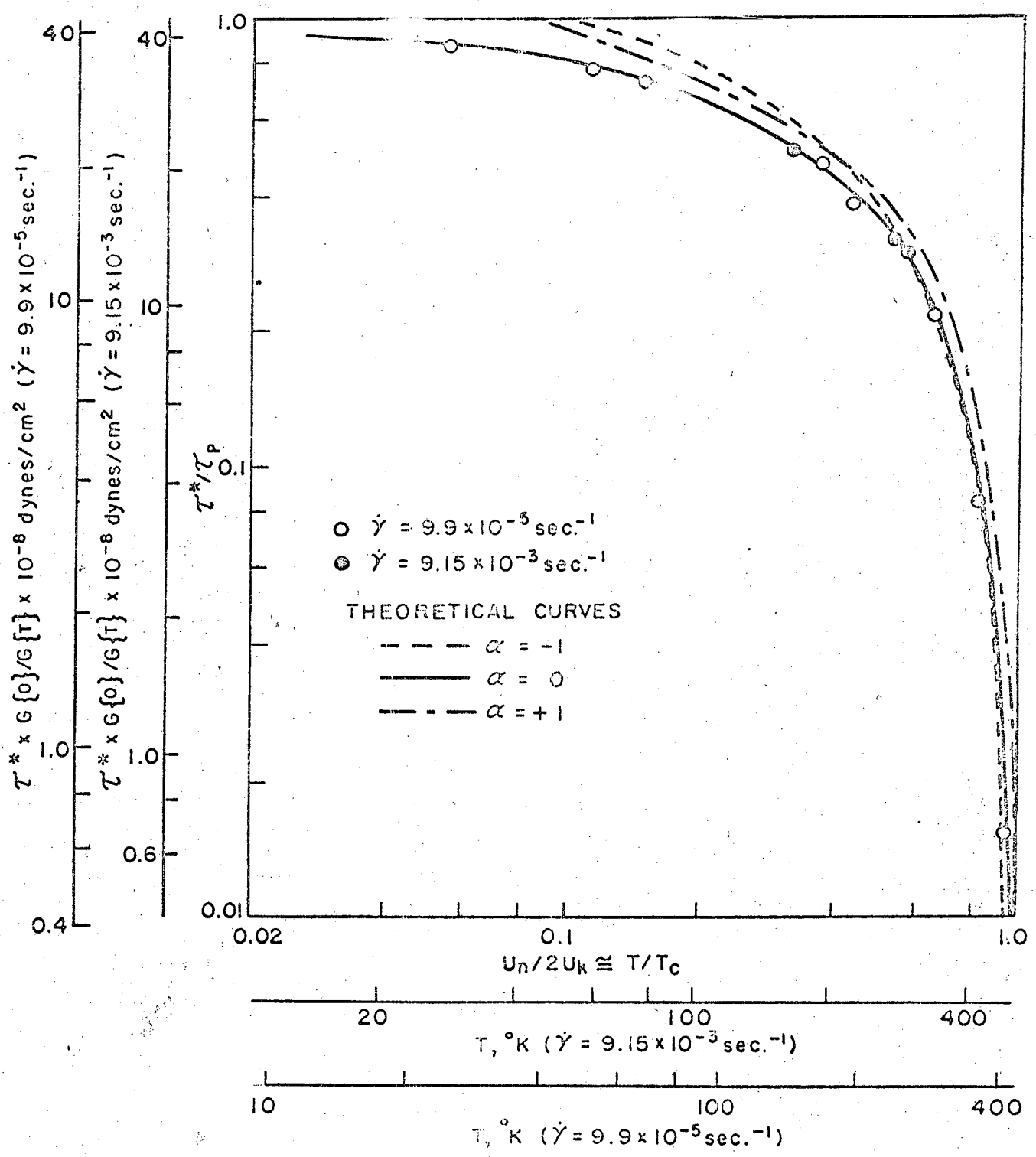

FIG. 7A. THE THERMALLY ACTIVATED FLOW STRESS vs. TEMPERATURE IN DIMENSIONLESS UNITS, FOR Mo.

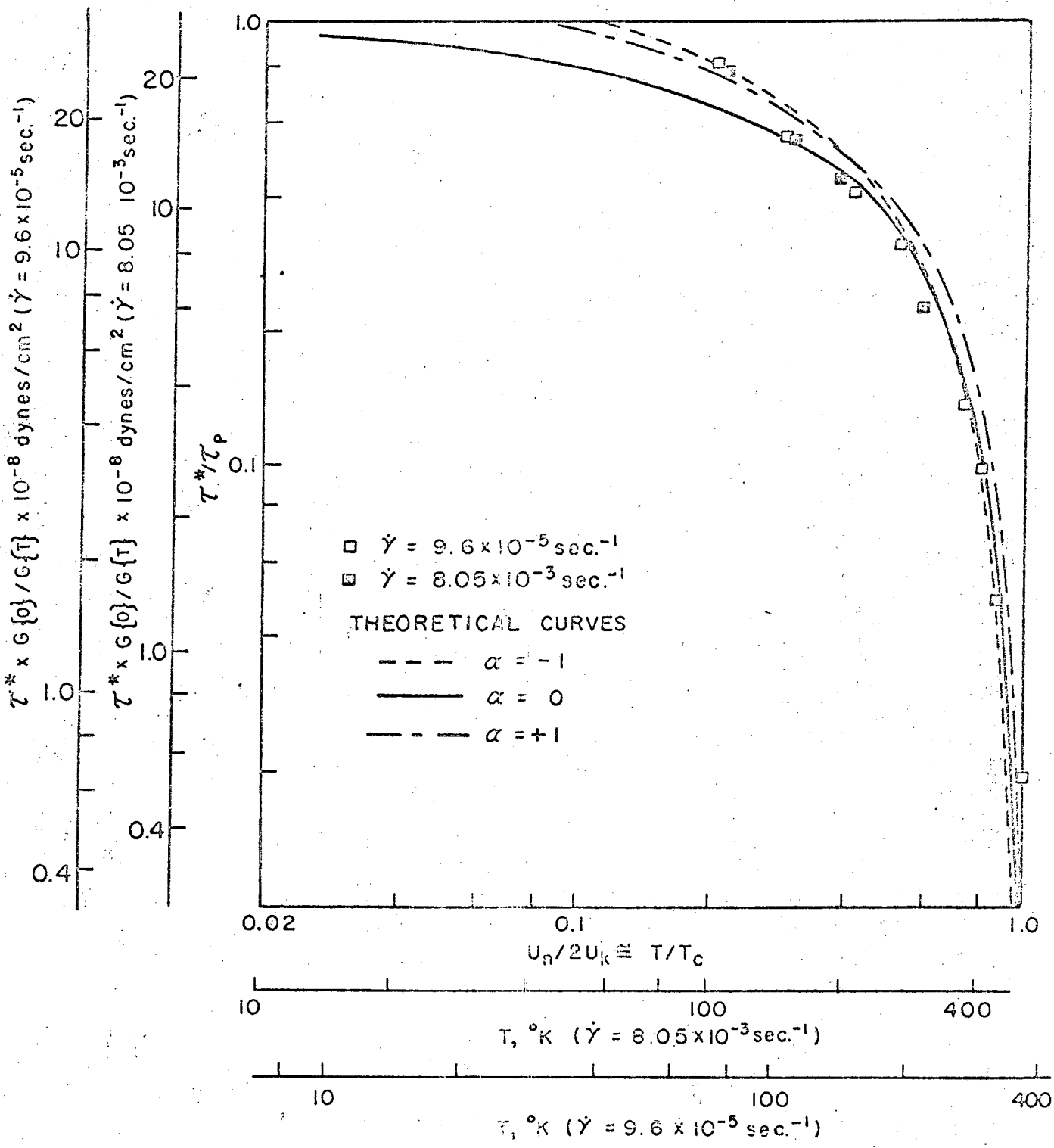

FIG. 7B. THE THERMALLY ACTIVATED FLOW STRESS vs. TEMPERATURE IN DIMENSIONLESS UNITS, FOR Ta.

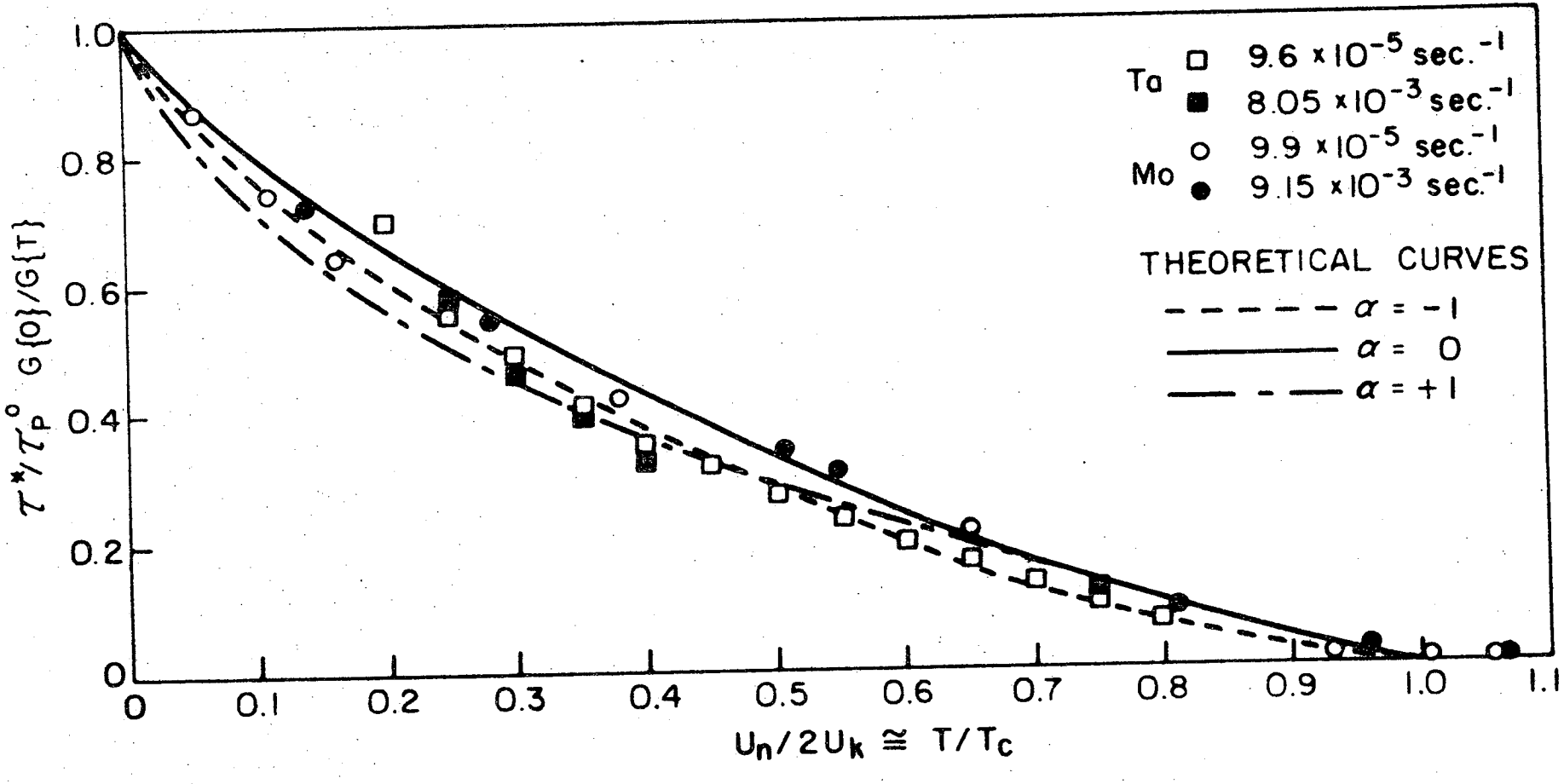

FIG. 8. THE THERMALLY ACTIVATED FLOW STRESS vs. TEMPERATURE FOR Ta & Mo.

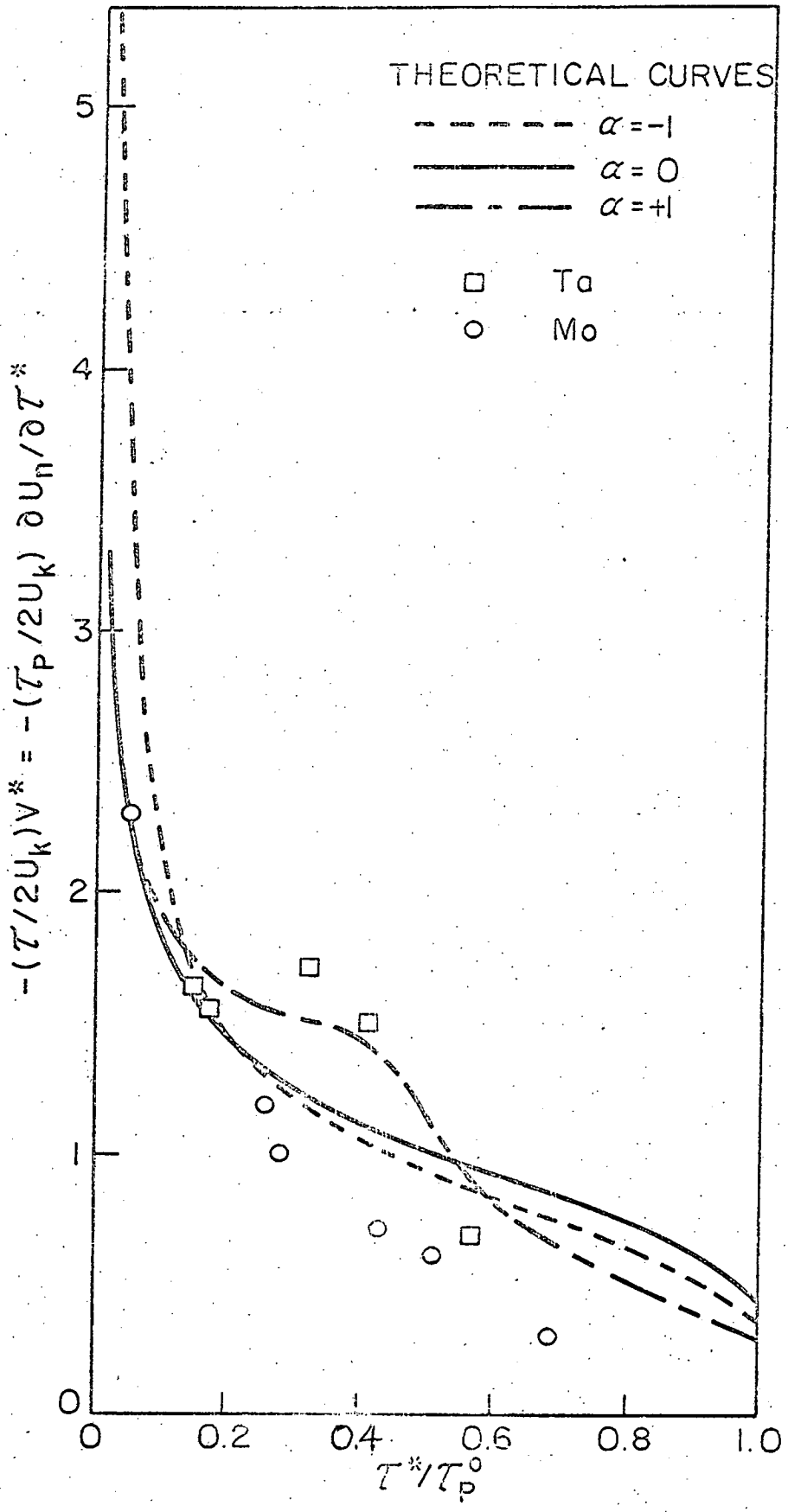

FIG. 9. THE THERMALLY ACTIVATED COMPONENT OF FLOW STRESS vs. ACTIVATION VOLUME IN DIMENSIONLESS TIME FOR Ta AND Mo.

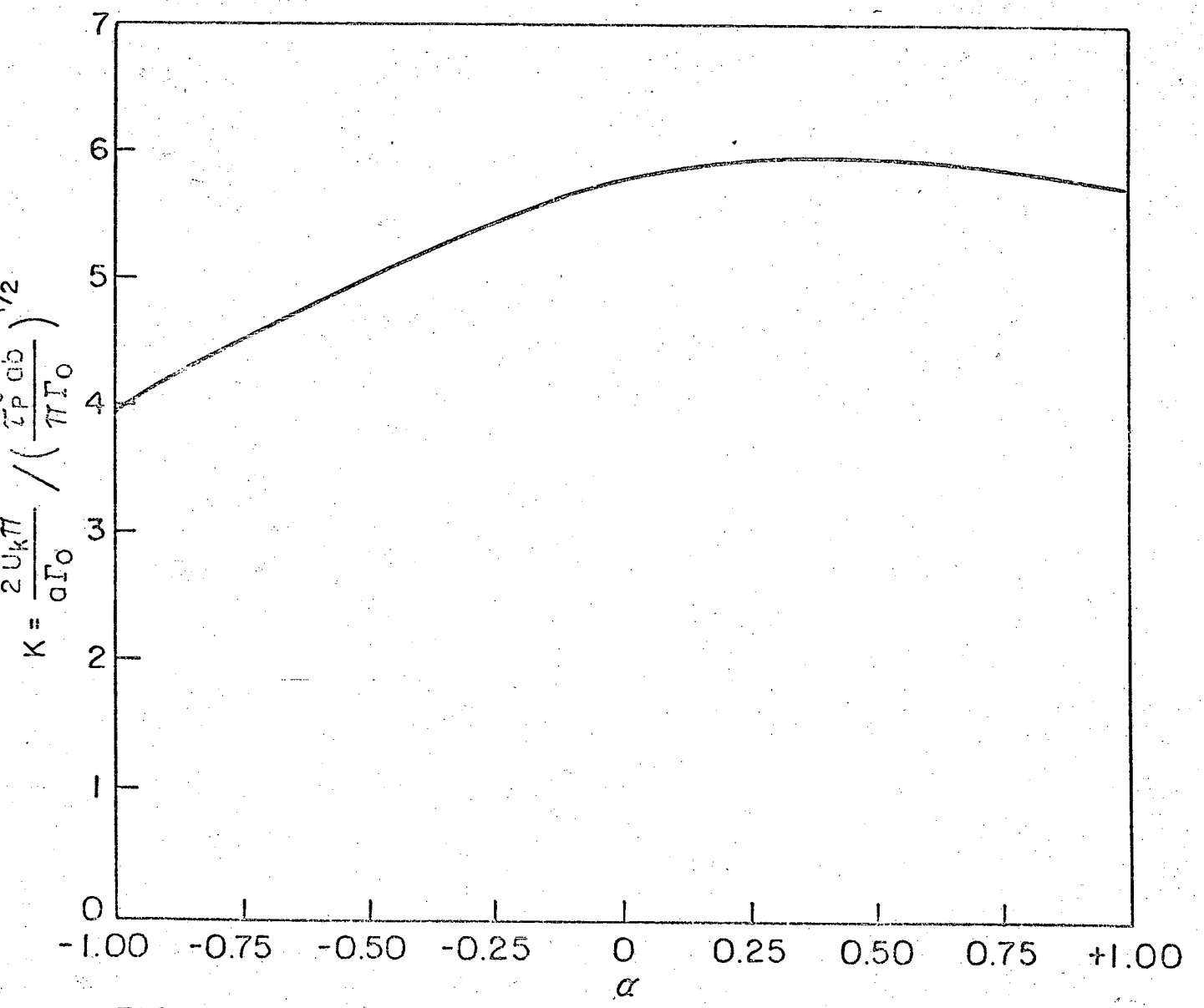

FIG. 10. VARIATION OF K WITH α FOR NUCLEATION OF DISLOCATION KINKS.